International Journal of Bioprinting

RESEARCH ARTICLE

# Preparation and characterization of 3D-printed antibacterial hydrogel with benzyl isothiocyanate

**Yunxia Liang[1†], Bimal Chitrakar[2†], Zhenbin Liu[1], Xujia Ming[1], Dan Xu[1], Haizhen Mo[1], Chunyang Shi[1], Xiaolin Zhu[1], Liangbin Hu[1*], Hongbo Li[1*]**

[1]School of Food Science and Engineering, Shaanxi University of Science and Technology, Xi'an, 710021, China

[2]College of Food Science and Technology, Hebei Agricultural University, Baoding, 071001, Hebei, China

(This article belongs to the *Special Issue: Related to 3D printing technology and materials*)

## Abstract

Benzyl isothiocyanate (BITC) is an isothiocyanate of plant origin, especially the mustard family, which has good antibacterial properties. However, its applications are challenging due to its poor water solubility and chemical instability. We used food hydrocolloids, including xanthan gum, locust bean gum, konjac glucomannan, and carrageenan as three-dimensional (3D)-printing food ink base and successfully prepared 3D-printed BITC antibacterial hydrogel (BITC-XLKC-Gel). The characterization and fabrication procedure of BITC-XLKC-Gel was studied. The results show that BITC-XLKC-Gel hydrogel has better mechanical properties by low-field nuclear magnetic resonance (LF-NMR), mechanical properties, and rheometer analysis. The strain rate of BITC-XLKC-Gel hydrogel is 76.5%, which is better than that of human skin. Scanning electron microscope (SEM) analysis showed that BITC-XLKC-Gel has uniform pore size and provides a good carrier environment for BITC carriers. In addition, BITC-XLKC-Gel has good 3D-printing performance, and 3D printing can be used for customizing patterns. Finally, inhibition zone analysis showed that the BITC-XLKC-Gel added with 0.6% BITC had strong antibacterial activity against *Staphylococcus aureus* and the BITC-XLKC-Gel added with 0.4% BITC had strong antibacterial activity against *Escherichia coli*. Antibacterial wound dressing has always been considered essential in burn wound healing. In experiments that simulated burn infection, BITC-XLKC-Gel showed good antimicrobial activity against methicillin-resistant *S. aureus*. BITC-XLKC-Gel is a good 3D-printing food ink attributed to strong plasticity, high safety profile, and good antibacterial performance and has great application prospects.

***Keywords:*** Antibacterial hydrogel; Benzyl isothiocyanate; 3D printing; Rheological properties; *Staphylococcus aureus*; *Escherichia coli*

†These authors contributed equally to this work.

***Corresponding authors:**
Liangbin Hu
(hulb@sust.edu.cn)
Hongbo Li
(hongbo715@163.com)

**Citation:** Liang Y, Chitrakar B, Liu Z, 2023, Preparation and characterization of 3D-printed antibacterial hydrogel with benzyl isothiocyanate. *Int J Bioprint*, 9(2): 671.
https://doi.org/10.18063/ijb.v9i2.671

**Received:** September 9, 2022

**Accepted:** November 8, 2022

**Published Online:** January 17, 2023



## 1. Introduction

Benzyl isothiocyanate (BITC) is an isothiocyanate of plant origin, which has good antibacterial properties[1]. BITC is potentially beneficial to human health. It is widely found

in *Alliaria petiolata*, water cress, garden cress, and papaya seeds[2]. It exerts a broad spectrum of antibacterial activities against a range of pathogens, including *Escherichia coli*, *Staphylococcus aureus*, *Bacillus subtilis*, and *Aspergillus niger*[3]. Among them, an excellent inhibitory effect was observed against *S. aureus* ATCC25923 and methicillin-resistant *S. aureus* (MRSA)[4]. BITC is a novel potential bacteriostatic agent against human infections[5]. However, BTIC has strong volatility, diminishing its antibacterial activities and hindering its potential use[6]. To solve this problem, some researchers have used cyclodextrin-coated hydrogels to improve its use and increase the antibacterial function[7,8].

Burns are responsible for more than 300,000 deaths annually worldwide and infection is a major cause of morbidity and mortality in these patients[9]. *E. coli* and *S. aureus* are among the most common pathogens of burn infections[10]. *S. aureus* causative agent is relatively pathogenic to humans and is found on the skin and mucosa of up to 40% of all population. Burn injuries are infected with *S. aureus* in 30% of cases[11]. In addition, multidrug-resistant *S. aureus* has become a global public health concern. MRSA was once considered the most potent pathogens in intensive care units and burns worldwide[12]. Bacterial infection after burn is the main cause of poor wound healing, resulting in sepsis, disability, and even death[13]. At present, the mechanism of wound healing after burn is a dynamic and complex process, which relies heavily on wound dressings; the wound is normally covered to prevent infection[14]. Since the bacterial infection is the most common infection in wound dressings, the use of antibiotics has become the main focus. However, bacterial drug resistance resulted from the abuse of antibiotics has given rise to additional challenges[15]. Therefore, it is indispensable to explore safe, green, and environmentally friendly wound dressings with good hydrophilic three-dimensional (3D) porous structures, and biocompatibility and extracellular matrix (ECM) turn out to be the most competitive candidates for wound dressings and have attracted the interest of many researchers[16,17].

Traditional hydrogel dressings are usually prepared through chemical reactions using chemical substances. The disadvantage of these products is that they are often non-biodegradable and carry certain safety risks[18]. In recent years, xanthan gum (XG), locust bean gum (LBG), konjac glucomannan (KG), and carrageenan (CA) are often used as edible gums for the preparation of edible hydrogels[19-21]. However, a single edible gum may reduce the comprehensive mechanical properties of the hydrogel. To solve the problems of bioavailability of BITC and non-degradability and safety issues of conventional dressings, we used XG, LBG, KG, and CA in combination as raw materials to prepare 3D-printed safe natural composite hydrogel (BITC-XLKC-Gel) through physical crosslinking method to increase its comprehensive performance in this study. Its mechanical and antibacterial properties were also studied. We found that BITC hydrogels had better mechanical properties and excellent plasticity compared to single colloid product. Most importantly, BITC-XLKC-Gel exhibited excellent antibacterial properties against *S. aureus*. In this study, the BITC-XLKC-Gel prepared by physical crosslinking method is a kind of safe, green, and environment-friendly dressing. It reduces the volatilization of BITC and broadens the application space of BITC and has a good application prospect.

## 2. Materials and methods

### 2.1. Materials and strains

BITC was purchased from Yuanye Biology Co., Ltd. (Shanghai, China). Food-grade XG, LBG, KG, and CA were obtained from Qiansheng Biotechnology Co., Ltd. (Hebei, China). All chemicals, such as potassium bromide, sodium chloride, ethanol, and so on, were of analytical grade. *E. coli* (MG 1655), *S. aureus* (ATCC 25923), and MRSA were obtained from the China General Microbiological Culture Collection Center (Beijing, China).

### 2.2. Preparation of BITC hydrogels

Deionized water was added with different concentrations of edible gel (Table 1). The mixture was heated and stirred in a water bath of 70~90°C, then, 0.2%~0.8% BITC was added to the above mixed solution, stirred, and left for 20 min, and the BITC hydrogel was obtained by physical crosslinking. All hydrogels were prepared in at 4°C and stored in a refrigerator.

### 2.3. Rheological measurements

The rheological test was conducted using an MCR 301 rheometer (Anton Paar, Austria) following the method described by Li *et al.*[22] with slight modification. The elastic modulus (G') and viscous modulus (G") were measured at 25°C, taking 1 mL of the sample. For oscillatory temperature scanning test, the test temperature range

**Table 1. Different proportions of compound water gel formulations**

| Hydrogels | Xanthan gum (%) | Locust bean gum (%) | Konjac glucomannan (%) | Carrageenan (%) |
|---|---|---|---|---|
| X-Gel | 2% | / | / | / |
| XLC-Gel | 0.05% | 0.05% | / | 0.1% |
| XLK-Gel | 0.05% | 0.05% | 0.1% | / |
| XLKC-Gel | 0.05% | 0.05% | 0.1% | 0.1% |
| C-Gel | / | / | / | 1% |

used was 4 – 40°C; the rate of temperature change during heating and cooling was 0.03333°C/s; the frequency was 1 Hz. The G' and G" were recorded as a function of time. Each sample was measured in triplicate.

### 2.4. Texture profile analysis (TPA)

TPA of the gel samples was performed using a SMS-TA. XT PlusC texture analyzer (Stable Micro Systems Co., Ltd., UK). Since X-Gel is a liquid and cannot be detected, we determined the other four types of TPA. The hydrogels prepared were cut into 1.5 × 1.5 × 0.8 $cm^3$ blocks for the measurement of TPA. The TPA test parameters used were: Cylindrical probe (SMS p/75); the velocity before/during/after measurement was 1.00 mm/s; the strain rate was 30%; the strain time was 5 s; and the trigger force was 5.0 N. The measurements of each sample were obtained in triplicate.

The tensile property was tested using the method described by Ma *et al.*[23] using a A/MTG physical property analyzer (Stable Micro Systems Co., Ltd., UK). The hydrogel film was cut into 10 × 50 × 3 mm strip and sandwiched between the splints. The tensile test was performed at a speed of 3 mm/s until the film fracture breaks stopped.

### 2.5. Water distribution

Water distribution was measured using the method described by Yoon *et al.*[24] using a Niumag Benchtop NMR Analyzer PQ 001 (Suzhou Niumag Analytical Instrument Co., Ltd., Jiangsu, China). The hydrogel samples (3 g) were packed tightly in 2 mL vials (2 mL, 12×36 mm, borosilicate glass – HPLC automatic sampler) and were then placed in a magnetic chamber. The transverse relaxation time ($T_2$) was measured using Carr-Purcell-Meiboom-Gill (CPMG) pulse sequence. The test parameters used are as follows: Sampling frequency = 200 KHz; main frequency = 21 MHz; radio frequency delay = 0.02000 ms; frequency offset = 877243.25 Hz; analog gain = 20 dB; 90° pulse width = 7 μs; digital gain = 3; sampling points = 3,000,090; pre-release gear = 1; waiting time = 5000.000; cumulative number of times = 8; 180° pulse width = 13.52 μs; echo time = 1.00000 MS; and number of echoes = 15,000. Each measurement was obtained in triplicate.

### 2.6. 3D printing of different hydrogels

The 3D printing of different hydrogels was performed by SHINNOVE-D13D double nozzle printer (Hangzhou Shiyin Technology Co., Ltd.). The printing parameters are as follows: Printing temperature was 80°C; nozzle diameter was 0.8 mm; material filling ratio was 100%; printing speed was 25 mm/s; and layer height was 3 mm. 3D-printing characteristics of hydrogels with different compositions were studied.

### 2.7. SEM analysis

The hydrogel morphology was observed under a scanning electron microscope (JSM-6510, Japanese electronics). The samples were freeze-dried before the test and the test voltage was 20 kV[25].

### 2.8. Antibacterial activity of the BITC hydrogel

*E. coli* MG1655 and *S. aureus* ATCC25923 strains were cultured overnight in lysogeny broth (LB) and Trypticase Soy Broth (TSB) at 37°C with swirling at 200 rpm[26]. The overnight cultures were serially diluted to approximately $10^7$ CFU/mL using the corresponding culture media. The diluted cultures (200 μL) were evenly spread over the agar plate of the culture medium, and then, BITC additions of 0% (control), 0.4%, 0.6%, and 0.8% hydrogels (BITC-XLKC-Gel) were placed on the surface of the solid media. After 24 h in 37°C incubator, the diameter of inhibition zone was measured to compare the inhibition effect. The growth inhibition zone of the hydrogel showed that the hydrogel exerted antibacterial activity after 24 h of incubation at 37°C[27].

To investigate the scavenging activity of BITC hydrogel on biofilm of *S. aureus* and *E. coli*, TSB or LB (100 μL) was taken into the well of 96-well polystyrene microplate and the culture medium containing *S. aureus* or *E. coli* (10 μL) was separately added. Then, the BITC-XLKC-Gel added with 0, 0.2, 0.6, and 0.8% BITC was added. The group without bacterial solution and hydrogel was used as the blank and incubated at 37°C for 36 h. After biofilm formation, 200 μL sterile phosphate-buffered saline (PBS) was added to each well after the medium was aspirated and the gel blocks were removed, and the plate wells were washed 3 times. Then, 100 μL 1% crystal violet solution was added to each hole, and biofilm was dyed at room temperature for 15 min. After aspirating the crystal violet staining solution in the culture medium, the excess dye was rinsed off with running water[28], and the plates were inverted on the filter paper to remove residual water and then dried in an oven at 37°C or at room temperature. After complete drying, 100 μL of 33% glacial acetic acid was added to each hole and placed in a 37°C incubator for 30 min to dissolve crystal violet. The optical density (OD) of the solution in the culture well was measured at 595 nm. The test was repeated for 3 times for each strain to obtain average value. The culture medium without inoculated bacteria was used as the negative control[29].

### 2.9. Experimental study on the effect of the hydrogel on the infection of porcine skin after burn

The effect of hydrogel on the skin infection of post-burn pigs was studied according to Lin *et al.*[30]. The pigskin was cut into 2.5 × 3 $cm^2$ pieces and soaked in 75% alcohol to remove

bacteria on the surface. Then, the surface was burned over flame for 30 s, and *S. aureus* strain ATCC25923 and MRSA were cultured overnight in TSB at 37°C with swirling at 200 rpm. The overnight culture was serially diluted to about $10^7$ CFU/mL using the appropriate medium. The diluted bacterial solution (40 μL) was evenly coated onto the surface of the burned pig skin. Thereafter, hydrogels containing different concentrations of BITC (0, 0.2, 0.6, and 0.8%) were applied on the pigskin. After incubation at 37°C for 16 h, the culture was removed and washed using PBS, and the culture was centrifuged at 8000 ×g at 25°C for 5 min. The precipitates were dissolved in 1 mL of PBS; diluted 10 times in a 96-well plate; and then, 4 μL of mixed drops were transferred onto the plate containing TSB. The diluent was placed on *S. aureus* counter plate to measure *S. aureus* colonies. The plates were incubated at 37°C for 12 h and *S. aureus* colonies were counted manually.

### 2.10. Statistical analysis

All experiments were performed in triplicate. Excel 2003 and Origin 8.5 were used for drawing figures and data processing. Analysis of variance (ANOVA) of the data collected was performed to determine the significant difference among the means. $P < 0.05$ was considered statistically significant.

## 3. Results and discussion

### 3.1. Rheological properties of the hydrogels with different compositions

The viscosity of the hydrogels with different compositions at 25°C is shown in Figure 1A. As shear stress increased, the viscosity of the hydrogels decreased gradually and became stable after 40 r/1/s, while the viscosity of the XLC-Gel, XLK-Gel, and XLKC-Gel liquid improved, but the difference was not significant. Among them, XLK-Gel liquid had the best viscosity, which was consistent with the shear thinning characteristics of XG. The X-Gel and C-Gel showed relatively poor levels of viscosity.

The storage modulus (G') and loss modulus (G") of hydrogels are shown in Figure 1B and C. For the study of hydrogels, dynamic rheological data can be used to evaluate gelation and gel formation, reflecting related physical and chemical properties of the composite hydrogels. The structural formation of macromolecules can be explained through the determination of viscoelasticity using dynamic measurements, where the elasticity is expressed as the energy storage modulus G' and the viscosity is expressed as the loss modulus G"[31]. In the relationship between G', G", and frequency shown in Figure 1B and 1C, the modulus of G' and G" of hydrogels increased slightly with the increase of frequency, while the G' and G" modulus of the hydrogels, X-Gel, and C-Gel increased rapidly. Within the frequency range, the value of G' of all hydrogels is much higher than the value of G", and the results showed that all hydrogels had a stable structure and good viscoelasticity. On the whole, the G' of the XLKC-Gel produced the largest G", which was significantly higher than that of other hydrogels. This indicated that the XLKC-Gel hydrogel had better viscoelastic properties than the other hydrogels. This also indicates that the addition of XG, LBG, KG, and CA can maximize the rheological properties of the hydrogels. Therefore, we chose to use the XLKC-Gel hydrogel to further study the effect of temperature change on the viscoelasticity (G' and G") of the gel (Figure 1D). Whether it was heating up or cooling down, there was no overlap between G' and G". This indicates that the gelation of XLKC-Gel occurs at 4~40°C and remains solid all the time[32]. With the increase of temperature, the value of G› decreases gradually, and the value of G› is much higher than that of G" in the range of 4~40°C, it shows that the XLKC-Gel composite hydrogel has good elasticity.

### 3.2. Mechanical properties of hydrogels with different compositions

TPA is one of the most widely used testing methods for measuring the texture characteristics of hydrogels, including hardness, adhesiveness, cohesiveness, stickiness, elasticity, and resilience. These parameters quantitatively characterize the mechanical properties of the hydrogels. The texture characteristics of the hydrogel with different components are shown in Figure 2. Elasticity is the ratio of the height of the deformed sample to the height before deformation after the removal of pressure and is expressed as the ratio of the height of the second compression to that of the first compression. Cohesion is the relative resistance of the sample to second compression following first compression and refers to the size of the internal binding force required to form the sample shape; it reflects the strength of the combination between the molecules or the structural elements of the sample. The larger the number, the greater the cohesion, and the stronger the ability of the sample to resist damage and maintain its integrity. Figure 2A and F shows that the XLC-Gel, XLK-Gel, XLKC-Gel, and C-Gel hydrogels have good elasticity and cohesiveness, which indicate the gelation level of the hydrogels.

Hardness is the ability of a material to resist local plastic deformation due to mechanical indentation or wear. Macroscopic hardness indicates the presence of strong molecular bonds, but the behavior of solid materials is complex under the action of external forces. As shown in Figure 2D, the hardness of the compound, XLKC-Gel, was

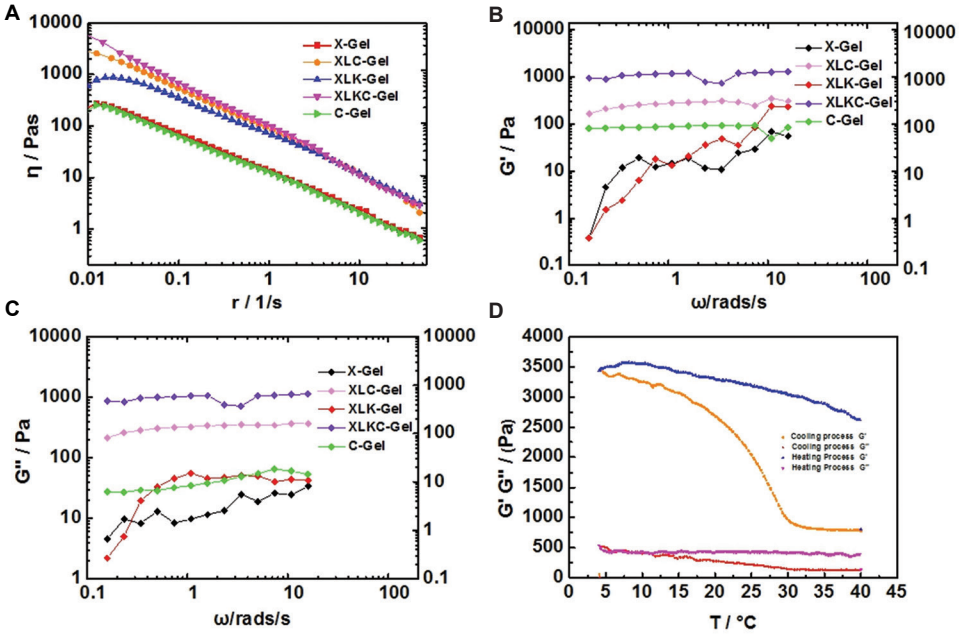


**Figure 1.** Rheological properties of hydrogel. (A) The relationship between viscosity and the shear rate of the gels. (B) Graph of the elastic modulus (G'[Pa]) and angular velocity. (C) Graph of the loss modulus (G"[Pa]) and angular velocity. (D) The influence of the elastic modulus (G'[Pa]) and loss modulus (G"[Pa]) of the XLKC-Gel as a function of temperature (4 – 40°C).

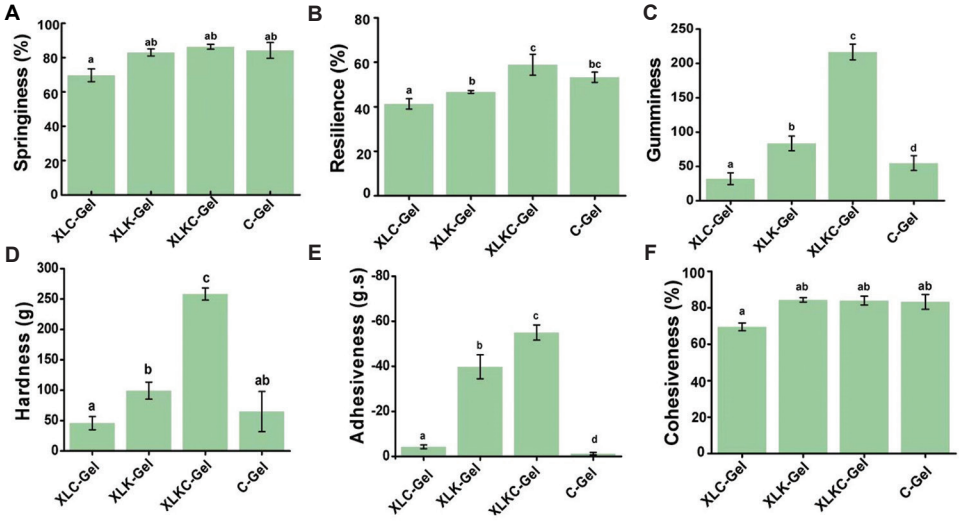


**Figure 2.** Texture analysis of hydrogel. (A) Springiness. (B) Resilience. (C) Gumminess. (D) Hardness. (E) Adhesiveness. (F) Cohesiveness.

the highest and was 3 – 4 times higher than that of other gels, which can be explained through comparison with other viscose compositions. The hardness value of XLKC is also higher than that of the hyaluronic acid carboxymethyl cellulose hydrogel prepared by other researchers[33]. The composite hydrogel containing XG, LBG, KG, and CA showed better hardness. Adhesion is the force of attraction between different molecules, while stickiness refers to the nature or state of a substance that is sticky; both of them are manifestations of viscosity. As shown in Figure 2C and E, the adhesiveness resulting from adding KG to XLK-Gel was higher than adding the same to XLC-Gel. This can be explained by the fact that KG can increase the viscosity of the gel. The gumminess and adhesiveness of the XLKC-Gel hydrogel were much higher than that of other hydrogels, which indicate that the compound hydrogel containing four types of hydrocolloids in combination can form a better gel system. In the resilience test (Figure 2B), the compound hydrogel, XLKC-Gel, had the best resilience, which was confirmed by the improved gel properties of

the compound hydrogels containing XG, LBG, KG, and CA. Compared with the hyaluronic acid carboxymethyl cellulose hydrogel prepared by other researchers, the adhesiveness of X hydrogel is −47.5 g.s, which is higher than that of hyaluronic acid carboxymethyl cellulose hydrogel. The resilience is 60%, which is lower than that of hyaluronic acid carboxymethyl cellulose hydrogel[33]. Therefore, compared with hydrogels prepared by chemical crosslinking method, XLKC-Gel has lower resilience, which may be a disadvantage of hydrogels prepared by physical crosslinking method. However, in terms of safety of the preparation materials, XLKC-Gel prepared by edible colloid is safer than hydrogels prepared by chemical crosslinking.

For skin wound repair materials, tearing wound dressings applied on to especially the injuries of frequently active joints can also be a potential risk for infection. Therefore, having suitable mechanical properties similar to those of skin is beneficial in maintaining the integrity of the material[34]. The tensile stress and strain of the four hydrogels are shown in Figure 3A, and among the four hydrogel samples, the breaking elongation of the CA-only-added C-Gel was only 24.6%. The breaking elongation of XLK-Gel at 58.5% was superior to that of XLC-Gel at 36.8%, and it could be explained by the addition of KG increasing the viscoelasticity of XLK-Gel, thus increasing its ductility. The XLKC-Gel hydrogel has a breaking elongation of 76.5%, which is much higher than that of the other three hydrogels and is superior to 60 – 75% of that of human skin[35]. The tensile stress of four hydrogels increased from 15.1 KPa and 29.7 KPa to 60.4 KPa and 83.3 KPa, and the maximum stress of XLKC-Gel was higher than that of other three hydrogels. The mechanical properties of XLKC-Gel are better than those of the other three groups. The results showed that the composite gel with XG, LBG, KG, and CA had better gel properties. The XLKC-Gel has good adhesive properties and can adhere firmly to the sloping skin surface and the curved joints of the hand, and it does not move with the movement of the hand. Therefore, XLKC-Gel is more suitable for skin wound dressings attributed to its excellent extensibility and adhesion.

### 3.3. Moisture distribution of the different hydrogels

Low-field nuclear magnetic resonance (LF-NMR) mainly reflects the law of water migration at different states of the hydrogel using relaxation time (T2). The horizontal coordinate in the water distribution map shows relaxation time, which indicates the fluidity of water in the hydrogel, and the vertical coordinate shows signal intensity (proton density), which indicates the water content corresponding to relaxation time. The transverse relaxation time of 1 – 10 ms shows $T_{2b}$, representing strong binding of water in the gel. Similarly, the transverse relaxation time of 10 – 100 ms shows $T_{21}$, representing the weak binding of water in the gel, while that of 100 – 1000 ms shows $T_{22}$, which represents easily flowing water in the gel, and 1000 – 10000 ms shows $T_{23}$, which represents free water in the gel.

In general, the relaxation time of the gel is inversely proportional to the binding degree of water molecules. The longer the relaxation time, the higher the degree of freedom of water. The shorter the relaxation time ($T_2$), the more tightly the binding of water to the substrate, and the better the water retention ability. The longer the relaxation time ($T_2$), the looser the water binding to the substrate, and the more free the water molecules are, while the poorer the water retention ability[36-38]. As shown in Figure 3B and Table 2, most of the water in the gels were primarily at $T_{22}$ (water that does not flow easily) and $T_{23}$ (free water), together accounting for more than 90%, while others were at $T_{2b}$ and $T_{21}$ (strong and weak binding water), with bound water showing strong interactions with specific groups of polymers, such as hydroxyl or ester groups, while intermediate bound water interacts weakly with polymers, which is usually the water bound by polymer networks. There was no significant interaction between free water and polymers[39].

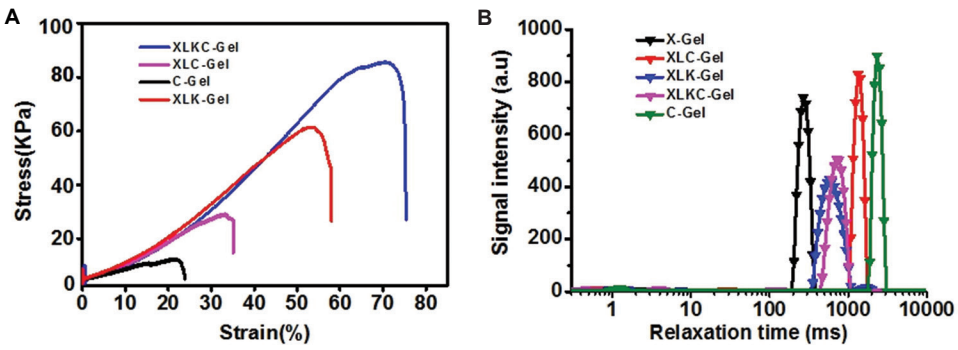


**Figure 3.** Tensile properties and water distribution of hydrogels. (A) Stress-strain curves of the hydrogel. (B) Water distribution of the hydrogel.

As shown in Figure 3B and Table 2, the peak area ratio of $T_{22}$ (water that is not easy to flow) of the hydrogel with only XG was 98.971%, indicating that XG has a strong water retention capacity, in other words, increased polymer gel network of water binding. XLC-Gel and C-Gel are hydrogels containing CA. The peak area ratios of $T_{23}$ (free water) are 96.976% and 98.494%, indicating that the water formed by CA is free water, which is unstable, easy to run off, and has low water holding capacity. From the comparison of XLC-Gel and XLKC-Gel hydrogels, it can be seen that KG can increase the water-holding capacity of the gel. Thus, for XLC-Gel and XLKC-Gel, although the same amount of CA was added to both, XLKC-Gel had stronger water retention due to the addition of KG to XLKC-Gel. First, the stronger the water-holding capacity, the stronger the ability to keep the wound moist, and thus, a physical barrier can be better formed to resist the effect of microbial contamination of the wound. Second, the stronger the water retention capacity, the stronger the hydrogel can support, thus enhancing its printability. It can be concluded that the interaction of XG, LBG, KG, and CA can increase the water-binding capacity of the polymer gel network. Thus, the XLKC-Gel system's high water retention capacity protects the wound from microbial contamination and improves the printability of the hydrogel.

**Table 2. Proportion of peak area of water in different states of hydrogel (%)**

| Hydrogels | $T_{2b\ (1\sim10\ ms)}$ | $T_{21\ (10\sim100\ ms)}$ | $T_{22\ (100\sim1000\ ms)}$ | $T_{23\ (1000\sim10000\ ms)}$ |
|---|---|---|---|---|
| X-Gel | 1.029% | / | 98.971% | / |
| XLC-Gel | 2.656% | 0.548% | / | 96.976% |
| XLK-Gel | 2.124% | / | 96.352% | / |
| XLKC-Gel | 2.665% | / | 97.336% | / |
| C-Gel | 1.506% | / | / | 98.494% |

### 3.4. Plasticity analysis of different hydrogels

To evaluate the 3D-printing adaptability of hydrogels, we performed 3D printing of different hydrogels and screened the optimal formulation combination of hydrogels. The 3D-printed models of the different hydrogels are shown in Figure 4A. The printed butterfly model was selected to evaluate the 3D-printing performance and the supporting performance of the four hydrogels. The X-gel cannot be printed because it is liquid and has no gel-forming property when heated. Among the other four hydrogels, the XLKC-Gel had the best 3D-printing formability and support in terms of printability and appearance. Furthermore, the printed lines were clear and the model was complete. This was consistent with previous rheological and texture results. Combined with the previous results of rheology, texture, and LF-NMR moisture distribution, XLKC-Gel showed the best comprehensive performance, and results of 3D printing revealed that it had the best formability and plasticity. Therefore, we chose XLKC-Gel as the carrier to embed BITC, to follow-up as a burn dressing application. In addition, the materials used in XLKC-Gel are natural, edible, and safe. XLKC-Gel can be used to print many models, such as cherry blossom, rabbit, bear, and starfish (Figure 4B), and can be used for 3D printing of burn dressings. One advantage of 3D-printed XLKC-Gel is that it can be printed in customized shapes on irregular skin surfaces for use as wound dressings.

### 3.5. SEM characterization

The morphologies of XLKC-Gel and BITC-XLKC-Gel were analyzed using SEM. As shown in Figure 5, the network structure of the gel was very obvious. At 500×, it was observed that the surface of the gel was relatively flat and uniform, while at 100× (100 μm), it was observed that the surface of the BITC-XLKC-Gel has many spherical particles oozing from the surface, whereas the surface of XLKC-Gel does not

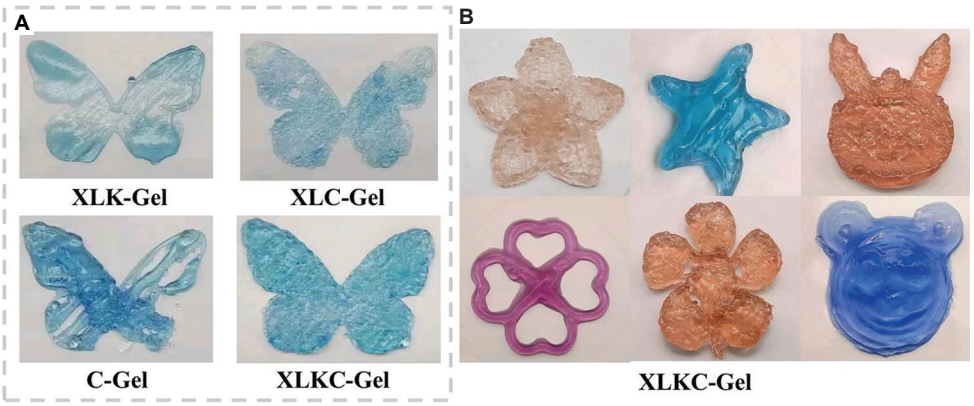


**Figure 4.** Three-dimensional (3D)-printed models of different hydrogel. (A) Comparison of 3D-printing performance of different hydrogel. (B) The 3D-printing model of XLKC-Gel.

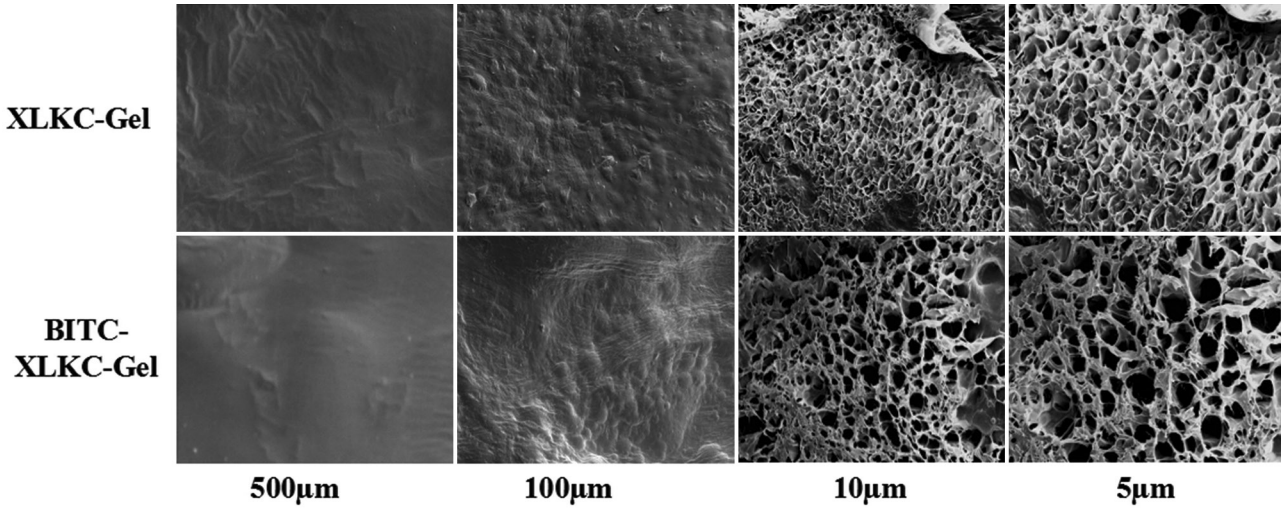


**Figure 5.** The scanning electron microscope images of XLKC-Gel and benzyl isothiocyanate-XLKC-Gel.

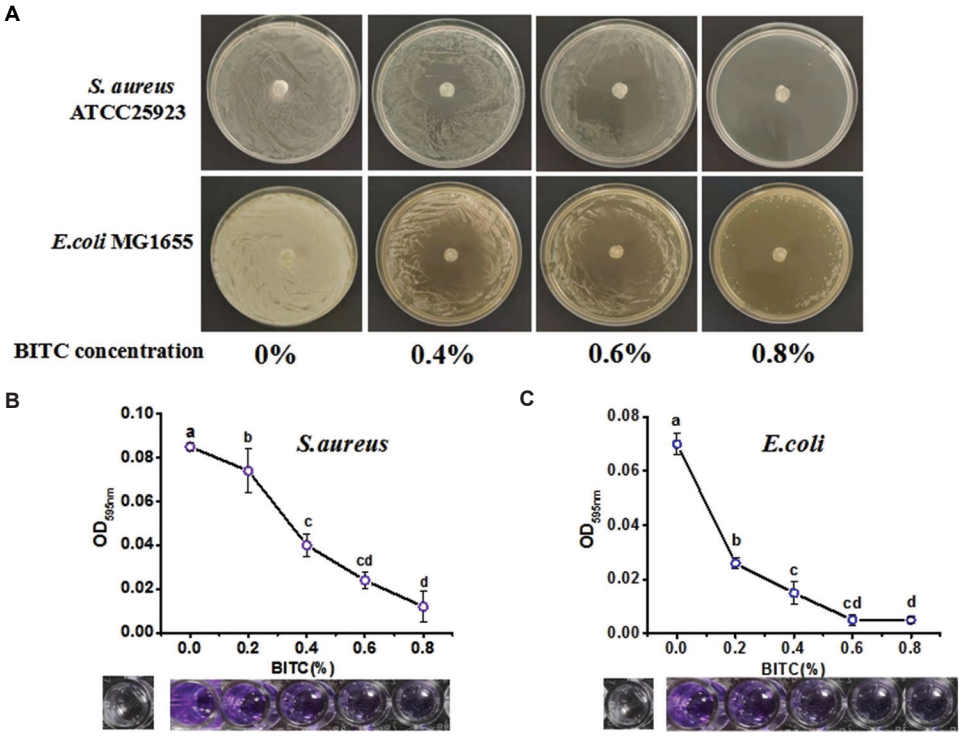


**Figure 6.** Antibacterial activity of the benzyl isothiocyanate (BITC) hydrogel against *Staphylococcus aureus* and *Escherichia coli*. (A) Bacteriostatic zone test of hydrogel. (B) Inhibitory effect of BITC hydrogel on *E. coli* biofilms. (C) Inhibitory effect of BITC hydrogel on *S. aureus* biofilms.

have such a morphology. These spheres can be regarded as BITC embedded in the gel after XG emulsion. In addition, we observed a clear reticular structure at 10× (10 μm) and 5× (5 μm) in the hydrogels, XLKC-Gel and BITC-XLKC-Gel, and the reticular structure was evenly distributed. The pore size of the network structure was favorable for the release of BITC and also for sustained release. BITC-XLKC-Gel had a larger pore size at the same field of view, compared with XLKC-Gel. This indicates that the addition of BITC could increase the pore size of hydrogel, providing a suitable environment for its subsequent use as a delivery carrier of polymer drugs.

### 3.6. Antibacterial activity of the BITC hydrogel

We used *S. aureus* to evaluate the antibacterial activity of the BITC hydrogel. *S. aureus* is a kind of Gram-positive bacteria

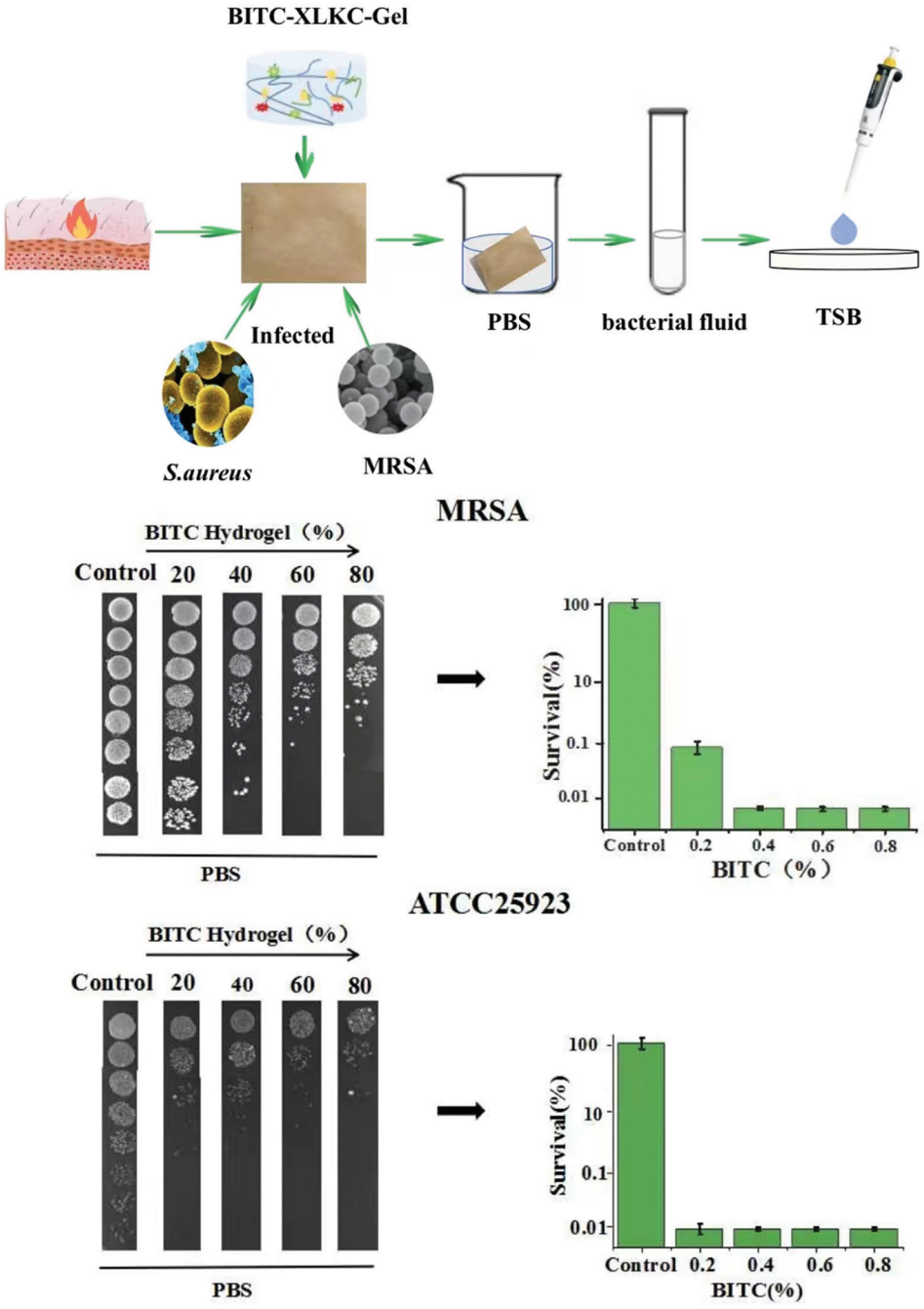


**Figure 7.** Minimum bactericidal concentration of benzyl isothiocyanate hydrogel against *Staphylococcus aureus* ATCC25923 and methicillin-resistant *S. aureus.*

that cause post-burn infection[40]. *E. coli* is the most common Gram-negative burn pathogen[41]. The antibacterial activity of the BITC hydrogel against *S. aureus* ATCC25923 and *E. coli* MG1655 is shown in Figure 6A, while Table 3 shows the size of the inhibition zone. Compared with the solid agar plate containing LB and the solid agar plate containing TSB, there was no inhibition zone on the agar plate without BITC (0% BITC concentration) and the whole plate was full of *E. coli* MG1655 and *S. aureus* ATCC25923. When the BITC concentration of the BITC hydrogel was 0.4%, 0.6%, and 0.8%, the inhibition regions formed on both the solid agar plate containing LB and the solid agar plate containing TSB, while the diameter of the inhibition zone increased from 1.5 cm to 6 cm (Table 3). The larger the

**Table 3. BITC hydrogel for *S. aureus* and *E. coli* bacteriostatic zone diameter**

| Strain | Diameter of bacteriostatic zone/cm | | | |
|---|---|---|---|---|
| | 0% (control) | 0.4% | 0.6% | 0.8% |
| *E. coli* MG1655 | 0 | 1.5 | 3.2 | 6 |
| *S. aureus* ATCC25923 | 0 | 2.0 | 3.8 | 5.8 |

*E. coli: Escherichia coli, S. aureus: Staphylococcus aureus*, BITC: Benzyl isothiocyanate

inhibitory region, the better the antibacterial property of the BITC-XLKC-Gel. Therefore, the results showed that BITC-XLKC-Gel with BITC had a good antibacterial effect on both *S. aureus* and *E. coli*.

Bacterial biofilms are a unique form of bacterial survival, compared to a single dispersed planktonic cell[42]. Bacterial biofilms refer to the capsular biota composed of polysaccharides, proteins, and nucleic acids secreted by bacteria on the surface of mucosa or biomaterials and the formation of biofilm is the main cause of chronic infection[43]. According to statistics, about 65% of human bacterial infections are caused by bacterial biofilms[44]. Therefore, to better evaluate the antibacterial performance of BITC hydrogel, we studied the effect of BITC-XLKC-Gel on the formation of biofilm of *S. aureus* and *E. coli* (Figure 6B and C). BITC-XLKC-Gel induced the lysis of *S. aureus* ATCC25923 and *E. coli* MG1655 cells, prevented the formation of biofilm, and reduced the established biofilm of *S. aureus* and *E. coli*. Quantitative analysis of crystal violet showed that when the addition of BITC was 0.2% and 0.4%, the treatment significantly reduced the ability of *E. coli* and *S. aureus* to form biofilms, while 0.6% and 0.8% BITC almost completely eliminated the ability of *S. aureus* to form biofilms (Figure 6B and C). This is consistent with the results of the bacteriostatic circles (Figure 6A). In summary, 0.4% BITC added BITC-XLKC-Gel showed good antibacterial activity against *E. coli* and *S. aureus*.

### 3.7. Experiments of infection on pig skin burn

Burns are one of the most destructive and common types of injuries. Severe thermal injury can result in an immunosuppressive state that predisposes burn patients to infectious complications[45]. Infection is the most common cause of death among burn patients. The longer the burn patient is treated, the higher the risk of infection caused by multidrug-resistant bacterial pathogens. In the first few days after a burn, the burn patient is more susceptible to infection by Gram-positive bacteria; therefore, active infection control methods are essential[46]. *S. aureus* is the main causative agent of infection in critically ill patients[47], with MRSA being the most infectious Gram-positive bacteria among burn patients[48].

Pigskin has a wide range of mechanical properties and tissue similar to human skin tissue and is often used as a biomechanical model of body skin tissue substitute to simulate human skin[49]. To evaluate the efficacy of the antibacterial properties of the BITC hydrogel for the treatment of bacterial infections on burned skin, we used pigskin as a model to simulate human skin burn by burning pigskin over flame. The standard *S. aureus* strains ATCC25923 and MRSA were used, then BITC-XLKC-Gel of different concentration was applied to the surface of burned skin, and the bacteriostatic effect was observed after incubation at 37°C for 24 h. As shown in Figure 7, after 24 h of application of the hydrogel, the moisture content of skin tissue at the burn site of the pigskin increased, which can be explained by the good water retention ability of the hydrogel. The colony growth of *S. aureus* ATCC25923 and MRSA after application of the BITC hydrogel is shown in Figure 7. When the BITC concentration was 0.2%, the survival rate of *S. aureus* ATCC25923 and MRSA was lower than 0.1%. When the BITC concentration was 0.4%, 0.6%, or 0.8%, the survival rate of *S. aureus* ATCC25923 and MRSA was lower than 0.01%, and the BITC hydrogel exerted a better antibacterial effect on *S. aureus* ATCC25923 than on MRSA. The results showed that the BITC hydrogel exerted good antibacterial activity against *S. aureus* and MRSA. Therefore, the BITC hydrogel has great potential for use as a dressing for the treatment of bacterial infections on burned skin.

## 4. Conclusion

In this study, a 3D printable BITC-XLKC-Gel was prepared with XG/LBG/KG/CA as substrate, and its therapeutic effect on skin burn was studied. The printed product was found to be safe, convenient, and effective for skin burn dressing. The manufacturing process was simple, and the materials were safe for use. The BITC-XLKC-Gel was shown to have good mechanical properties, rheological properties, and water retention properties and showed great overall potential in the treatment of wound healing. The strain rate of BITC hydrogel is 76.5%, which is superior to human skin and has good adhesion and extensibility. In addition, inhibition zone analysis showed that the BITC-XLKC-Gel added with 0.6% BITC exerted strong antibacterial activity against *S. aureus* and the BITC-XLKC-Gel added with 0.4% BITC exerted strong antibacterial activity against *E. coli*. In the experiment that simulated burns and infections, BITC hydrogels showed excellent antibacterial properties against MRSA. In this study, we only investigated the antibacterial properties of the BITC hydrogel, while the active molecules involved in the healing process remain to be explored. In this study, we developed an edible, 3D-printed BITC hydrogel with strong plasticity, which has a good application prospect.

## Acknowledgments

None.

## Funding

This work is financially supported by the National Natural Science Foundation of China (Grant No. 31901795), the Basic Research Plan of the Education Department of Shaanxi (14Jk1086), and the Key R&D Program of Shaanxi, China (Grant No. 2021NY-157 and 2020NY-136).

## Conflict of interest

The authors declare no conflicts of interest.

## Author contributions

*Conceptualization:* Hongbo Li
*Investigation:* Dan Xu, Chunyang Shi, and Xiaolin Zhu
*Formal analysis and Methodology:* Yunxia Liang and Xujia Ming
*Project administration and Resources:* Haizhen Mo and Liangbin Hu
*Writing – original draft:* Yunxia Liang and Bimal Chitrakar
*Writing – review and editing:* Hongbo Li and Zhenbin Liu
*Funding acquisition:* Hongbo Li and Chunyang Shi

## Ethics approval and consent to participate

This article does not contain any studies involving human or animal subjects.

## Consent for publication

Not applicable.

## Availability of data

Not applicable.

## References

1. Wu X, Zhou QH, Xu K, 2009, Are isothiocyanates potential anti-cancer drugs? *Acta Pharmacol Sin*, 30: 501–512.

   https://doi.org/10.1038/aps.2009.50

2. Nakamura Y, Yoshimoto M, Murata Y, *et al.*, 2007, Papaya seed represents a rich source of biologically active isothiocyanate. *J Agric Food Chem*, 55: 4407–4413.

   https://doi.org/10.1021/jf070159w

3. Li P, Zhao YM, Wang C, *et al.*, 2021, Antibacterial activity and main action pathway of benzyl isothiocyanate extracted from papaya seeds. *J Food Sci*, 86: 169–176.

   https://doi.org/10.1111/1750-3841.15539

4. Li H, Ming X, Xu D, *et al.*, 2021, Transcriptome analysis and weighted gene co-expression network reveal multitarget-directed antibacterial mechanisms of benzyl isothiocyanate against *Staphylococcus aureus*. *J Agric Food Chem*, 69: 11733–11741.

   https://doi.org/10.1021/acs.jafc.1c03979

5. Romeo L, Iori R, Rollin P, *et al.*, 2018, Isothiocyanates: An overview of their antimicrobial activity against human infections. *Molecules*, 23: 624.

   https://doi.org/10.3390/molecules23030624

6. Uppal S, Kaur K, Kumar R, *et al.*, 2018, Chitosan nanoparticles as a biocompatible and efficient nanowagon for benzyl isothiocyanate. *Int J Biol Macromol*, 115: 18–28.

   https://doi.org/10.1016/j.ijbiomac.2018.04.036

7. Uppal S, Sharma P, Kumar R, *et al.*, 2020, Effect of benzyl isothiocyanate encapsulated biocompatible nanoemulsion prepared via ultrasonication on microbial strains and breast cancer cell line MDA MB 231. *Colloids Surf A Physicochem Eng Asp*, 596: 124732.

   https://doi.org/10.1016/j.colsurfa.2020.124732

8. Li W, Liu X, Yang Q, *et al.*, 2015, Preparation and characterization of inclusion complex of benzyl isothiocyanate extracted from papaya seed with β-cyclodextrin. *Food Chem*, 184: 99–104.

   https://doi.org/10.1016/j.foodchem.2015.03.091

9. Ramirez-Blanco CE, Ramirez-Rivero CE, Diaz-Martinez LA, *et al.*, 2017, Infection in burn patients in a referral center in Colombia. *Burns*, 43: 642–653.

   https://doi.org/10.1016/j.burns.2016.07.008

10. Keswani RK, Miglani OP, Sabherwai U, *et al.*, 1982, Infection in burn patients. *Burns*, 8: 256–262.

    https://doi.org/10.1016/0305-4179(82)90006-7

11. Bagdonas R, Tamelis A, Rimdeika R, 2003, *Staphylococcus aureus* infection in the surgery of burns. *Medicina* (*Kaunas*), 39: 1078–1081.

12. Lowy FD, 1998, *Staphylococcus aureus* infections. *N Engl J Med*, 339: 520–532.

    https://doi.org/10.1056/NEJM199808203390806

13. Ladhani HA, Yowler CJ, Claridge JA, 2021, Burn wound colonization, infection, and sepsis. *Surg Infect* (*Larchmt*), 22: 44–48.

    https://doi.org/10.1089/sur.2020.346

14. Lima T, Passos MF, 2021, Skin wounds, the healing process, and hydrogel-based wound dressings: A short review. *J Biomater Sci Polym Sci*, 32: 1910–1925.

    https://doi.org/10.1080/09205063.2021.1946461

15. Kopecki Z, 2021, Development of next-generation antimicrobial hydrogel dressing to combat burn wound infection. *Biosci Rep*, 41: BSR20203404.

    https://doi.org/10.1042/BSR20203404

16. Kamoun EA, Kenawy ES, Chen X, 2017, A review on polymeric hydrogel membranes for wound dressing applications: PVA-based hydrogel dressings. *J Adv Res*, 8: 217–233.

https://doi.org/10.1016/j.jare.2017.01.005

17. Kim H, 2018, Wound dressing materials: The essentials. *J Wound Manag Res*, 14: 141–142.

https://doi.org/10.22467/jwmr.2018.00458

18. Zhang M, Zhao X, 2020, Alginate hydrogel dressings for advanced wound management. *Int J Biol Macromol*, 162: 1414–1428.

https://doi.org/10.1016/j.ijbiomac.2020.07.311

19. Barak S, Mudgil D, 2014, Locust bean gum: Processing, properties and food applications--a review. *Int J Biol Macromol*, 66: 74–80.

https://doi.org/10.1016/j.ijbiomac.2014.02.017

20. Chen Y, Zhang M, Bhandari B, 2021, 3D printing of steak-like foods based on textured soybean protein. *Foods*, 10: 2011.

https://doi.org/10.3390/foods10092011

21. McKim JM, 2014, Food additive carrageenan: Part I: A critical review of carrageenan *in vitro* studies, potential pitfalls, and implications for human health and safety. *Crit Rev Toxicol*, 44: 211–243.

https://doi.org/10.3109/10408444.2013.861797

22. Li JQ, Geng S, Zhen SY, *et al.*, 2022, Fabrication and characterization of oil-in-water emulsions stabilized by whey protein isolate/phloridzin/sodium alginate ternary complex. *Food Hydrocolloids*, 129: 107625.

https://doi.org/10.1016/j.foodhyd.2022.107625

23. Ma W, Dong W, Zhao S, *et al.*, 2022, An injectable adhesive antibacterial hydrogel wound dressing for infected skin wounds. *Biomater Adv*, 134: 112584.

https://doi.org/10.1016/j.msec.2021.112584

24. Yoon WB, Gunasekaran S, Park JW, 2006, Characterization of thermorheological behavior of Alaska Pollock and Pacific whiting surimi. *J Food Sci*, 69: 338–343.

https://doi.org/10.1111/j.1365-2621.2004.tb13639.x

25. Zou Q, Tian X, Luo S, *et al.*, 2021, Agarose composite hydrogel and PVA sacrificial materials for bioprinting large-scale, personalized face-like with nutrient networks. *Carbohydr Polym*, 269: 118222.

https://doi.org/10.1016/j.carbpol.2021.118222

26. Xiu H, Zhao H, Dai L, *et al.*, 2022, Robust and adhesive lignin hybrid hydrogel as an ultrasensitive sensor. *Int J Biol Macromol*, 213: 226–233.

https://doi.org/10.1016/j.ijbiomac.2022.05.168

27. Qi L, Wang Y, Chen B, *et al.*, 2021, *In vitro* bacteriostatic effects of polymyxin B combined with propofol medium and long chain fat emulsion injection against *Escherichia coli*. *Ann Palliat Med*, 10: 4687-4687.

https://doi.org/10.21037/apm-21-751

28. Chen H, Zhou Y, Zhou X, *et al.*, 2020, Dimethylaminododecyl methacrylate inhibits *Candida albicans* and oropharyngeal candidiasis in a pH-dependent manner. *Appl Microbiol Biotechnol*, 104:3585–3595.

https://doi.org/10.1007/s00253-020-10496-0

29. Liu J, Jiang J, Zong J, *et al.*, 2021, Antibacterial and anti-biofilm effects of fatty acids extract of dried *Lucilia sericata* larvae against *Staphylococcus aureus* and *Streptococcus pneumoniae in vitro*. *Nat Prod Res*, 35: 1702–1705.

https://doi.org/10.1080/14786419.2019.1627353

30. Lin S, Pei L, Zhang W, *et al.*, 2021, Chitosan-poloxamer-based thermosensitive hydrogels containing zinc gluconate/recombinant human epidermal growth factor benefit for antibacterial and wound healing. *Mater Sci Eng C Mater Biol Appl*, 130: 112450.

https://doi.org/10.1016/j.msec.2021.112450

31. Katoch A, Choudhury AR, 2020, Understanding the rheology of novel guar-gellan gum composite hydrogels. *Mater Lett*, 263: 127234.

https://doi.org/10.1016/j.matlet.2019.127234

32. Huang M, Mao Y, Li H, *et al.*, 2021, Kappa-carrageenan enhances the gelation and structural changes of egg yolk via electrostatic interactions with yolk protein. *Food Chem*, 360: 129972.

https://doi.org/10.1016/j.foodchem.2021.129972

33. Janarthanan G, Shin HS, Kim IG, *et al.*, 2020, Self-crosslinking hyaluronic acid-carboxymethylcellulose hydrogel enhances multilayered 3D-printed construct shape integrity and mechanical stability for soft tissue engineering. *Biofabrication*, 12: 045026.

https://doi.org/10.1088/1758-5090/aba2f7

34. Ma W, Zhou M, Dong W, *et al.*, 2021, A bi-layered scaffold of a poly (lactic-co-glycolic acid) nanofiber mat and an alginate-gelatin hydrogel for wound healing. *J Mater Chem B*, 9: 7492–7505.

https://doi.org/10.1039/d1tb01039e

35. Annabi N, Rana D, Sani S, *et al.*, 2017, Engineering a sprayable and elastic hydrogel adhesive with antimicrobial properties for wound healing. *Biomaterials*, 139, 229–243.

https://doi.org/10.1016/j.biomaterials.2017.05.011

36. Bertram HC, Engelsen SB, Busk, *et al.*, 2004, Water properties during cooking of pork studied by low-field NMR relaxation: Effects of curing and the RN(-)-gene. *Meat Sci*, 66: 437–446.

https://doi.org/10.1016/S0309-1740(03)00132-3

37. Pearce KL, Rosenvold K, Andersen HJ, *et al.*, 2011, Water distribution and mobility in meat during the conversion of muscle to meat and ageing and the impacts on fresh meat quality attributes--a review. *Meat Sci*, 89: 111–124.

https://doi.org/10.1016/j.meatsci.2011.04.007

38. Yang KC, Wu CC, Cheng YH, *et al.*, 2008, Chitosan/gelatin hydrogel prolonged the function of insulinoma/agarose microspheres *in vivo* during xenogenic transplantation. *Transplant Proc*, 40: 3623–3626.

https://doi.org/10.1016/j.transproceed.2008.06.092

39. Chen F, Chen C, Zhao D, *et al.*, 2020, On-line monitoring of the sol-gel transition temperature of thermosensitive chitosan/β-glycerophosphate hydrogels by low field NMR. *Carbohydr Polym*, 238: 116196.

https://doi.org/10.1016/j.carbpol.2020.116196

40. Kooistra-Smid AM, van Zanten E, Ott A, *et al.*, 2008, Prevention of *Staphylococcus aureus* burn wound colonization by nasal mupirocin. *Burns*, 34: 835–839.

https://doi.org/10.1016/j.burns.2007.09.011

41. Azzopardi EA, Azzopardi E, Camilleri L, *et al.*, 2014, Gram negative wound infection in hospitalised adult burn patients--systematic review and metanalysis-. *PloS One*, 9: e95042.

https://doi.org/10.1371/journal.pone.0095042

42. Venkatesan N, Perumal G, Doble M, 2015, Bacterial resistance in biofilm-associated bacteria. *Future Microbiol*, 10: 1743–1750.

https://doi.org/10.2217/fmb.15.69

43. Tu C, Wang Y, Yi L, *et al.*, 2019, Roles of signaling molecules in biofilm formation. *Sheng Wu Gong Cheng Xue Bao*, 35: 558–566.

https://doi.org/10.13345/j.cjb.180326

44. Del Pozo JL, 2018, Biofilm-related disease. *Expert Rev Anti Infect Ther*, 16: 51–65.

https://doi.org/10.1080/14787210.2018.1417036

45. Church D, Elsayed S, Reid O, *et al.*, 2006, Burn wound infections. *Clin Microbiol Rev*, 19: 403–434.

https://doi.org/10.1128/CMR.19.2.403-434.2006

46. Lachiewicz AM, Hauck CG, Weber DJ, *et al.*, 2017, Bacterial infections after burn injuries: Impact of multidrug resistance. *Clin Infect Dis*, 65: 2130–2136.

https://doi.org/10.1093/cid/cix682

47. Chen K, Lin S, Li P, *et al.*, 2018, Characterization of *Staphylococcus aureus* isolated from patients with burns in a regional burn center, Southeastern China. *BMC Infect Dis*, 18: 51.

https://doi.org/10.1186/s12879-018-2955-6

48. Reardon CM, Brown TP, Stephenson AJ, *et al.*, 1998, Methicillin-resistant *Staphylococcus aureus* in burns patients--why all the fuss? *Burns*, 24: 393–397.

https://doi.org/10.1016/s0305-4179(98)00036-9

49. Chanda A, 2018, Biomechanical modeling of human skin tissue surrogates. *Biomimetics* (*Basel*), 3: 18.

https://doi.org/10.3390/biomimetics3030018